# Surface structure of GaAs(2 5 11)

L. Geelhaar, Y. Temko, J. Márquez, P. Kratzer, and K. Jacobi*
*Fritz-Haber-Institut der Max-Planck-Gesellschaft, Faradayweg 4-6, D-14195 Berlin, Germany*
(Received 10 October 2001; published 27 March 2002)

GaAs samples with orientations vicinal to (2 5 11) within 1° were prepared by molecular beam epitaxy and analyzed *in situ* by scanning tunneling microscopy, low-energy electron diffraction, and reflection high-energy electron diffraction. In addition, first-principles electronic structure calculations were carried out. GaAs(2 5 11) is a stable surface whose orientation is located within the stereographic triangle. For a wide range of As-rich conditions a $(1\times1)$ reconstruction forms that is characterized by an inclined series of three As dimers and that fulfills the electron counting rule. The terrace size is limited only by the macroscopic off-orientation of the samples. The surface is perturbed by thin stripes of the nearby orientation (3 7 15). While the dangling bond densities of GaAs(2 5 11) and GaAs(3 7 15) are almost equal, GaAs(3 7 15) violates the electron counting rule. The analysis of this perturbation suggests that, in general, on semiconductor surfaces the gain in stability arising from the minimization of the number of dangling bonds is significantly greater than the gain arising from reaching a semiconducting ground state. Upon annealing of the samples in ultrahigh vacuum, a fairly rough surface structure develops whose mean orientation is different from (2 5 11).

DOI: 10.1103/PhysRevB.65.155308 PACS number(s): 68.35.Bs, 81.05.Ea, 61.50.Ah, 68.37.Ef

## I. INTRODUCTION

Surfaces of single crystals can be divided according to their orientation into low-index and high-index surfaces. These names stem from the values of the respective Miller indices. In this context, low means usually 0 or 1. For example, for the diamond and zinc-blende lattices, and specifically for GaAs, the low-index surfaces are {001}, {011}, and {111}. Low-index surfaces are characterized by high crystal symmetry. Along these planes the bulk crystal forms stable, low-energy surfaces. In contrast, high-index surfaces are generally expected to be unstable and to decay into facets of low-index orientation. For this reason, low-index surfaces have been used in the vast majority of surface studies and semiconductor devices. However, in this paper we report on the surface structure of GaAs(2 5 11), a stable surface that is oriented far away from all low-index surfaces.

In recent years the interest in high-index semiconductor surfaces has markedly increased. This is mostly due to the rapidly expanding field of low-dimensional semiconductor structures like quantum wires and quantum dots, that are technologically very promising.[1] In particular, heterostructures made from III-V semiconductors are expected to lead to improved lasers,[2] and the prototype of these materials is GaAs. Because of their quantum nature, the properties of these low-dimensional structures are significantly influenced by their size and shape. Thus the analysis and the control of these parameters are of utmost importance. Facets of high-index orientation have been observed to form naturally on such structures.[3–6] The study of the respective planar surfaces is essential to validate the interpretation of the experimental data on the quantum structures and to model these structures.

Also, the study of high-index surfaces increases the general understanding of surface structures. On the basis of the abundance of data on low-index surfaces, guiding principles have been developed that describe the structure of semiconductor surfaces,[7] e.g., the electron counting rule (ECR).[8] The necessarily more complex structures of high-index surfaces offer the possibility to verify the generality of these principles. In addition, on high-index surfaces new structural motifs may occur, like the zigzag chain of arsenic dimers on GaAs(113)A–$(8\times1)$.[9–11]

A third motivation for the study of high-index surfaces is their potential as substrates for semiconductor devices. The performance of such devices depends on the orientation and the resulting properties of the substrate. For example, on GaAs(113)A quantum wires[12] and quantum dots[13] of excellent quality have been created by a method that cannot be employed on the standard substrate GaAs(001). Therefore the discovery of a new stable surface may open up the possibility to grow new types of heterostructures.

Zinc-blende-type crystals found in nature display only few facet orientations. This observation is usually discussed in the context of the equilibrium crystal shape. In thermodynamic equilibrium, a given amount of crystalline material takes on the shape that minimizes its free energy. The thus defined equilibrium crystal shape is determined by the free surface energy $\gamma$ of the various crystalline facets. This was realized long ago, and the relation between crystal shape and surface free energies is expressed in rigorous terms by the Wulff construction.[14] In a polar plot of the surface free energy as a function of orientation, orientations for which low-energy surface structures exist appear as minima. In the typical case of positive step energies, these minima form inward cusps in the polar plot of $\gamma$ (the so-called Wulff plot). For a typical covalent material, the Wulff construction yields the result that only few such minima with the lowest surface free energies determine the equilibrium crystal shape completely. These correspond to the well-known low-index surfaces. However, the surface energy at zero temperature is expected to display additional local minima. Furthermore, we note that full equilibration is often hampered by insufficient mass transport on the surface. For a crystal cut in a certain direction, mass transport is required to obtain a local orientation different from the average long-range orientation of the sur-

 

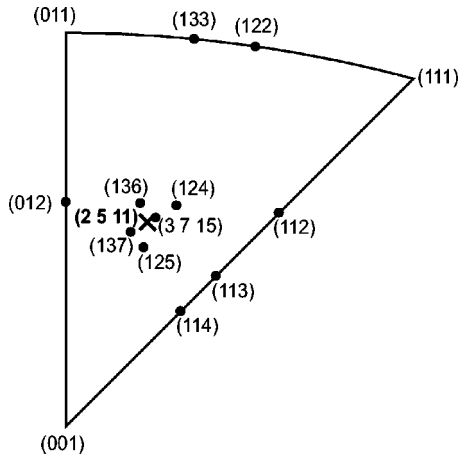


FIG. 1. Stereographic triangle. The orientations of the high-index GaAs surfaces studied and of facets, observed on InAs/GaAs(001) quantum dots, are indicated by filled circles. The orientation of the GaAs(2 5 11) surface is indicated by a cross.

face $\Theta$, determined by the cut. If the orientation of the surface corresponds to a *local* minimum in the Wulff plot, the surface is at least metastable. However, if there are other surface orientations $\Theta_i$ nearby with lower surface free energies $\gamma_i$, the surface prepared by cutting the crystal may undergo faceting upon annealing. In the simplest case, the equilibrium shape of the surface will consist of macroscopically large facets of two different orientations $\Theta_i, i=1,2$ arranged in such a way as to retain the average orientation $\Theta$ over large distances. This will occur if the surface free energy of the prepared surface is sufficiently high, $\gamma\Sigma_i\cot(\Theta-\Theta_i) > \Sigma_i\gamma_i\csc(\Theta-\Theta_i)$. In the opposite case, if no combination of *nearby* facets fulfilling the above inequality exists, we call the surface stable. It can be used as a substrate for crystal growth without risking that faceting will occur during deposition. This notion of stability will be used throughout in this paper. Thus epitaxy on high-index surfaces allows us to access surfaces that are relatively stable in the above sense, independent of their absolute stability as facets of crystals formed in equilibrium. We just note briefly that similar conclusions can be made for nanofacets of heteroepitaxial crystallites, because epitaxial strain as well as non-negligible contributions from the edges between adjacent facets contribute to the energy balance in these systems.

For graphical representation, it is easier to work with a stereographic projection of the orientation vector onto a plane, rather than with the three-dimensional vector itself. Because of the crystallographic symmetry, some orientations are equivalent. Hence it is sufficient to restrict this projection to the triangle whose corners are marked by the three low-index surfaces (001), (011), and (111) (cf. Fig. 1). However, for a polar material such as GaAs, *A* and *B* faces must be distinguished, i.e., one in principle needs to consider two separate stereographic triangles. Here, we restrict ourselves to *A* faces. A physical interpretation of the representation using the stereographic triangle can be given if we assume for the moment that surface atoms remain at their bulk positions. In this case, we can think of a surface of arbitrary orientation as being built up from atomic-scale units of the basic orientations (001), (011), and (111). A surface with orientation at an edge of the stereographic triangle is composed of the two low-index surfaces at the respective corners. All other surfaces are thought to be composed from all three low-index surfaces, and hence are more complex. However, for a stable singular surface, the above decomposition is merely a hypothetical concept.

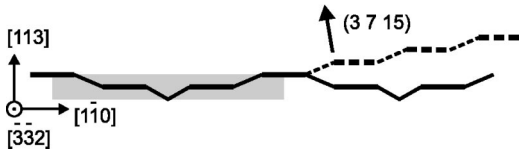


FIG. 2. Schematic cross section of the GaAs(113)*A*–$(8\times1)$ reconstruction (solid line). The gray rectangle indicates the width of the unit mesh. The zigzag chains of As dimers extend perpendicularly to the plane of drawing and are represented by the thick horizontal bars. Continuous stacking of such zigzag chains yields the plane (3 7 15) (dashed line).

A few of the GaAs surfaces on the edges have been studied. GaAs(113)*A*,[9–11,15] GaAs($\overline{113}$)*B*,[16,17] GaAs(114)*A*,[18–20] and GaAs($\overline{114}$)*B* (Ref. 19) are stable, and the structures of GaAs(113)*A*–$(8\times1)$ (Ref. 10) and GaAs(114)*A*–$\alpha2(2\times1)$ (Ref. 20) have been determined by first-principles calculations. GaAs(112)*A*,[10,21,22,27] GaAs($\overline{112}$)*B*,[10,27] GaAs(122)*A*,[23] GaAs(133)*A*,[22–25] GaAs($\overline{133}$)*B*[24] and GaAs(012)*A* (Refs. 22 and 26) are unstable. Surfaces that are located *within* the stereographic triangle have been reported only for elemental semiconductors [Si(123),[28] Si(137),[28] Ge(126),[29] Ge(1 8 16),[29] Ge(1 15 17),[30] Ge(3 15 23),[31,32] Ge(7 10 12),[32] and Ge(9 21 29) (Ref. 32)]. However, their structures have not been determined, and none of these studies was carried out on planar substrates of the respective orientation. Also, we note that there is generally no correspondence between the surface structure of elemental and compound semiconductors. The only exception is the (114) surface, where the same reconstruction was found for Si (Ref. 33) and GaAs.[20]

The first indications that there may be a stable GaAs surface within the stereographic triangle were found in our study on GaAs(112)*A*.[10,27] This surface decomposes into five facets of the orientations (111), {110}, (124), and (214). The latter two planes are equivalent and are located within the stereographic triangle (cf. Fig. 1). The occurrence of these facets suggested that the respective surfaces have a low surface energy and are stable. However, the orientation (124) was determined only with an experimental uncertainty of about 5°.

Further hints were based on the analysis of and experiments on GaAs(113)*A*–$(8\times1)$. This surface is composed of zigzag chains of arsenic dimers, and within the reconstruction the chains occur on two different levels (cf. Fig. 2). Thus there are stacks of two dimer chains diagonally on top of each other within a single terrace of this surface. Steps along these zigzag chains are very straight, and it was concluded that these zigzag chains are a very stable structural element.[11] Thus we speculated that a surface that is constructed by continuously stacking the zigzag chains (cf. Fig.

2) may also be stable. The orientation of this plane is (3 7 15). On a mesoscopic scale, GaAs(113)*A*–(8×1) is fairly rough. This roughness is accompanied by small regions whose mean orientation is not (113), and indeed facets of nanometer size of the orientation (3 7 15) have been observed on this surface.[34,35] (3 7 15) is also located within the stereographic triangle, and this orientation is in accord with the experimental data for the facets on GaAs(112)*A* as well.

Our quest for a stable GaAs surface within the stereographic triangle was additionally motivated by reports on the shape of InAs/GaAs(001) quantum dots that form by a self-organized process. Facets of the orientation {136} (Ref. 4) and (125) (Ref. 5) were found on these structures. These planes are located within the stereographic triangle, too. Since GaAs and InAs are very similar materials, these observations suggested as well that there may be a stable III-V semiconductor surface within the stereographic triangle. The occurrence of these facets was very surprising, because theoretical models for such quantum dots usually assume that their shape is dominated by low-index facets with low surface energy.[36] Therefore information on the respective planar surface within the stereographic triangle became even more important.

Experimental evidence that there is indeed a stable GaAs surface within the stereographic triangle was found in our study on spherical depressions that were ground into GaAs(113)*A* samples.[37] The diameter of these depressions was 3 mm, and their depth was 150 $\mu$m. Thus surfaces with an angle with respect to (113) of up to about 12° were created in all azimuthal directions. Low-energy electron diffraction (LEED) and scanning tunnel microscope (STM) images of a stable hitherto unknown surface were observed in a region of the depression that was off-oriented from (113) by $(9\pm2)°$ in direction $[1\bar{1}0]$. Due to experimental limitations, the exact orientation of that surface could not be determined. Hence it was at that time not possible to propose any structural model, either.

On the basis of this experimental proof, we carried out experiments on planar GaAs samples that were cut accordingly. The results from the depressions were confirmed, the Miller indices of the new stable GaAs surface within the stereographic triangle could now be identified as (2 5 11), and its atomic structure was determined.[38] With the help of these data, we were in another study able to determine unambiguously the orientation of the dominating bounding facets of InAs/GaAs(001) quantum dots as (137).[6] The discovery of the GaAs(2 5 11) surface has been described also elsewhere.[35] In the present paper, we shall supply additional data and a more detailed discussion of the surface structure of GaAs(2 5 11).

## II. METHODS

Experiments were carried out in a multichamber ultrahigh vacuum (UHV) system that has been described in detail elsewhere.[39] Samples approximately $10\times10$ mm$^2$ large were cut from two different wafers ($n$-type, Si-doped, carrier concentration $(1.1–4.8)\times10^{18}$ cm$^{-3}$, purchased from Wafer Technology) whose nominal orientations are (113) oriented by 9.7° and by 10.2°, respectively, in direction $[\bar{1}10]$ (manufacturer's specification); i.e., (3 7 15) and (19 47 99), or (2 5 11) off-oriented by 1° in direction $[19\,10\,\bar{8}]$ and by 1° in direction $[21\,40\bar{2}2]$, respectively. On the wafers the orientation of the projection of $[33\bar{2}]$ into the respective surface plane was indicated by the wafer manufacturer. This given direction was used for the structural analysis of the surface and is indicated for orientation in most images of experimental data. $[33\bar{2}]$ lies in the planes (113) and (3 7 15) (cf. Fig. 2). The angle between $[33\bar{2}]$ and (2 5 11) is 1.0°. After cleaning in propanol, samples were introduced into the UHV system via a loading chamber. After oxide desorption, samples were treated with several ion-bombardment and annealing (IBA) cycles. The annealing was carried out under $As_2$ flux at 580°C and yielded already diffraction patterns of fairly good quality. Subsequently, layers 20–400 nm thick were grown by molecular beam epitaxy (MBE). In the MBE chamber, the surface periodicity and quality was monitored by reflection high-energy electron diffraction (RHEED). The optimum surface quality was achieved at a growth temperature of 520–550°C and an $As_2$:Ga beam equivalent pressure ratio of 7–20. Afterwards, samples were kept under $As_2$ flux at a temperature of 450–460°C for 10–15 min. Different growth parameters resulted in the same surface structure, but at somewhat worse surface quality. For the second set of experiments, samples prepared in the aforementioned way were annealed in UHV at a temperature of up to 590°C for 5–15 min without $As_2$ flux. After preparation, samples were transferred *in situ* to the analysis chambers and characterized by low-energy electron diffraction (LEED) and scanning tunnel microscopy (STM). STM images were acquired in constant current mode.

Complementary to the experimental investigations, first-principles calculations using density-functional theory (DFT) were carried out in order to find the optimized atomic structure of the high-index surfaces under study. From the total-energy DFT calculations, absolute numbers of the surface energies were derived in order to assess the stability of these surfaces and to corroborate the correctness of the structural model suggested by previous experimental analysis. We used the pseudopotential/plane-wave approach for electronic structure calculations, as implemented in the computer code FHI98MD.[40] Norm-conserving pseudopotentials of Hamann type were constructed[41] for Ga and As, with the highest occupied *s* and *p* orbitals treated as valence states. The electronic exchange and correlation effects were treated within the local-density approximation.[42] The electronic wave functions were expanded into a set of plane waves. The convergence of this expansion was tested by comparing results for an energy cutoff of 10 and 15 Ry, and agreement of the surface energies to within 2 meV/Å$^2$ was assured. In our plane-wave approach, the surface is represented in a repeated-slab geometry, with a separation of adjacent slabs by a vaccuum region larger than 11 Å. Laterally, (1×1) unit meshs of the (2 5 11) and (3 7 15) surfaces with the theoretical bulk lattice constant of GaAs were used, and we started from the bonding topology suggested by experimental

STM images as input. One surface of the slab was passivated by pseudohydrogen atoms of two types, with fractional charges 3/4 and 5/4.[43] The dispersion of electronic bands was sampled using a Monkhorst-Pack *k*-point set[44] consisting of $(2\times4)$ *k* points in the entire surface Brillouin zone. Convergence tests for the slab thickness were performed using both 11- and 14-Å thick slabs (i.e., adding one monolayer of GaAs to the slab). The results showed that surface energies converged with respect to slab thickness to better than 1 meV/Å$^2$. The input coordinates of all atoms, apart from the hydrogen atoms and their bonding partners, were relaxed using the forces calculated self-consistently, until the remaining forces were smaller than 0.1 eV/Å. Simulated STM images were generated from the optimized structures by calculating and displaying the isosurfaces of a suitably defined local density of states. This procedure mimics experimental STM images acquired in constant current mode.[45]

In the following, we briefly describe the method used to obtain absolute surface energies of the relaxed structures. The first step, the calculation of the combined surface energy $\gamma_{comb}$ of both the clean and the hydrogen-passivated surface of the slab, is rather straightforward (see, e.g., Ref. 46). Let $N_{\mathrm{As}}$ and $N_{\mathrm{Ga}}$ be the number of As and Ga atoms in a unit mesh of the slab with area *A*, and $E_{slab}$ the cohesive energy of the slab (relative to isolated atoms). $\gamma_{comb}$ is obtained by subtracting from $E_{slab}$ a suitable amount of GaAs bulk material with cohesive energy $E^{coh}_{\mathrm{GaAs}}$ per formula unit,

$$\gamma_{comb}(\mu_{\mathrm{As}})=[E_{slab}-N_{\mathrm{Ga}}E^{coh}_{\mathrm{GaAs}}+(N_{\mathrm{As}}-N_{\mathrm{Ga}})\times(E^{coh}_{\mathrm{As}}-\mu_{\mathrm{As}})]/A. \quad (1)$$

We note that, for nonstoichiometric GaAs surfaces, i.e., when $N_{\mathrm{Ga}}\neq N_{\mathrm{As}}$, the surface free energy is a function of the chemical potential of one of the elements. In experiments, the dependence on chemical potential corresponds to a dependence of the surface preparation on temperature and Ga:As flux ratio. Here, we use the arsenic chemical potential $\mu_{\mathrm{As}}$ to account for this dependence. The cohesive energy of solid elemental arsenic $E^{coh}_{\mathrm{As}}$ constitutes an upper bound for $\mu_{\mathrm{As}}$ (see also Ref. 46). In the second step, we determine the energy of the hydrogen-passivated surface alone and subtract it from $\gamma_{comb}$. To this end, reference slabs with two hydrogen-terminated surfaces are constructed, which contain the same structural motifs (H–As–H groups, As–H groups, and Ga–H groups) as occur on the hydrogen-passivated (2 5 11) surface. Specifically, we use a GaAs(001) slab passivated with H(3/4) on both sides. Its absolute surface energy can be determined because its two surfaces are symmetry equivalent by virtue of a rotation-reflection axis. Thus a formula similar to Eq. (1) applies, but with an additional factor 1/2 in account of the two equivalent surfaces. In order to obtain reference energies for monohydride passivation groups, we employ a GaAs(001) slab with a pair of *A* steps on one surface, where the As atoms at the step carried passivating As–H groups. In a similar way, a reference slab with *B* steps and passivating Ga–H groups is prepared. Eventually, we obtain the surface energies of the clean high-index surfaces by subtracting out the energy contribution of their passivating hydride groups. The results are quoted together with the linear dependence on $\mu_{\mathrm{As}}$, $\gamma=\gamma_{\text{As-rich}}+\alpha(E^{coh}_{\mathrm{As}}-\mu_{\mathrm{As}})$. The linear coefficent $\alpha$ is determined by the surface stoichiometry $\Delta N_{\mathrm{As}}$, i.e., the number of As atoms per unit mesh that need to be added to a stoichiometric surface in order to build up the desired structure, according to the relation $\alpha=\Delta N_{\mathrm{As}}/A$.

## III. RESULTS AND DISCUSSION

### A. Atomic structure

A LEED image of GaAs(2 5 11) is shown in Fig. 3(a). The spots are arranged in an oblique net. This pattern is identical to the one that was observed in the spherical depression in GaAs(113)*A*.[37] This is evidence that the same stable surface is now found on a planar sample. The spots are sharp, which indicates a high surface quality. In contrast to LEED images of other stable high-index GaAs surfaces,[11,17,19] almost all the spots are visible. Two different unit meshes are marked in Fig. 3(a). Unit mesh *B* fulfills the rigorous crystallographic convention that the basis vectors be as short as possible, and was chosen in Ref. 37. However, in the course of the present study it turned out that the surface structure is described more intuitively by unit mesh *A*. Since the areas of both unit meshes are equal, the two unit meshes are equivalent. Thus in the following we will refer mostly to unit mesh *A*.

The reciprocal surface net is depicted schematically on the left-hand side of Fig. 3(b). The corresponding surface net in real space is constructed on the right-hand side of this figure. Note that none of the real-space basis vectors is parallel to any of the reciprocal space basis vectors, because the surface net is oblique. From the LEED data it was calculated that the lengths of the basis vectors of unit mesh *A* are in real space $(11.1\pm0.5)$ and $(21\pm1)$ Å, and the enclosed angle is $68°\pm2°$.

Characteristic RHEED images of GaAs(2 5 11) are presented in Fig. 3(c). These images appear if the electron beam is aligned along the three directions of high crystal symmetry that correspond to the basis vectors of the two unit meshes in real space. Thus one-dimensional cross sections of the reciprocal space surface net are acquired that are oriented perpendicular to the electron beam. The images were acquired at room temperature. During growth, RHEED patterns were basically identical but the background intensity was higher. For each direction, two RHEED images are shown that were taken at two different angles of incidence of the electrons. The specular streak is not necessarily the brightest one, and the intensities of the other streaks are not symmetrically distributed with respect to the specular streak. The latter observation indicates that the reconstruction is not symmetrical with respect to the plane defined by the electron beam and the surface normal. The diffraction streaks of the zero-order Laue circle are more pronounced for the greater angle of incidence. However, the relative intensities of the streaks within this circle are different than in the image for the smaller angle. This is most apparent in direction $[2\bar{3}1]$. At different angles of incidence the Ewald sphere intersects the rods of the reciprocal net at different heights. The change in

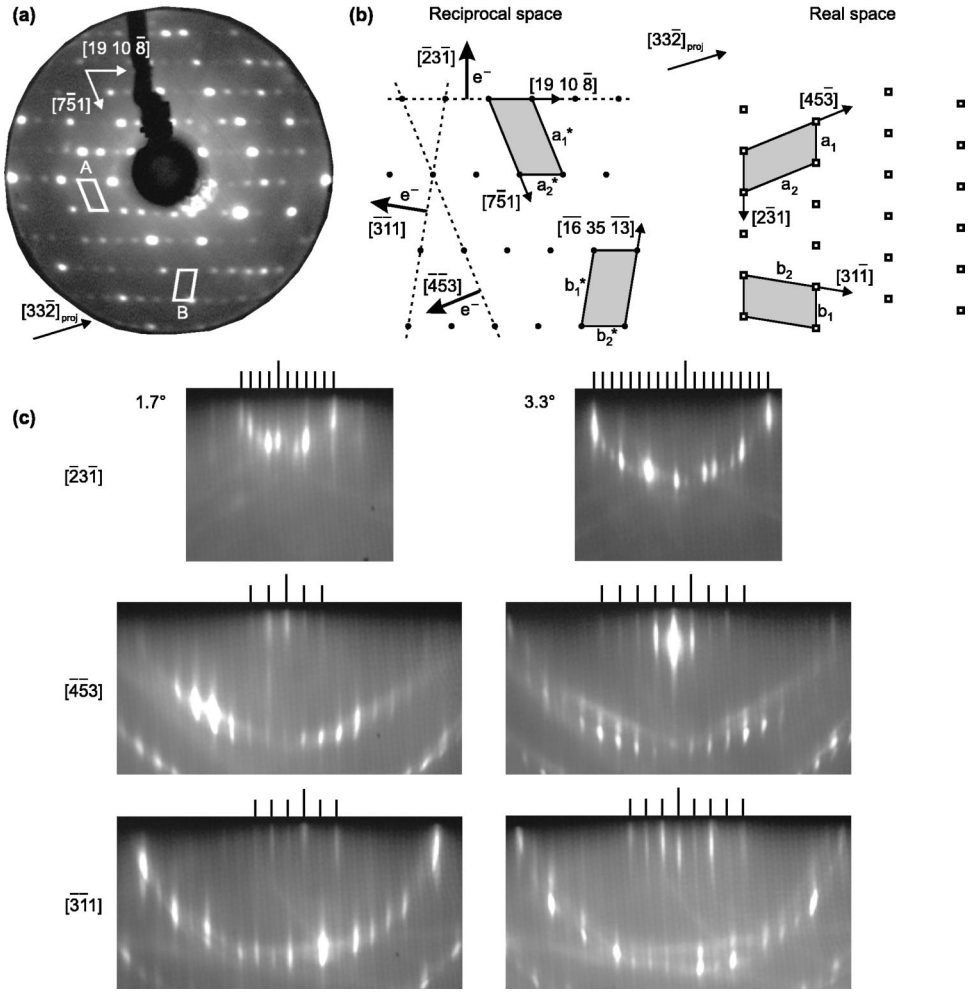


FIG. 3. (a) LEED image of GaAs(2 5 11). $E=59$ eV. (b) Schematic of the surface net in reciprocal space (left-hand side) and in real space (right-hand side). (c) RHEED images of GaAs(2 5 11). The vertical lines at the top of the images mark the positions of the diffraction streaks of the zero order Laue circle. The longest line is located for each image above the specular streak. The respective orientations of the electron beam are indicated on the left-hand side of the images. The angles of incidence are specified next to the images in direction $[\bar{2}3\bar{1}]$. The experimental uncertainty of the angles is $\pm 0.2°$. Because of the off-orientation of the samples, the actual angle of incidence with respect to the plane (2 5 11) is along $[\bar{4}5\bar{3}]$ and $[\bar{3}1\bar{1}]$ smaller by about 1°.

the relative intensities implies that the intensity varies along different rods perpendicular to the surface in a different way.

An overview STM image of GaAs(2 5 11) is shown in Fig. 4(a). Terraces vary considerably in size, with the largest ones extending over more than 1000 Å. There are basically no islands on the terraces. The region on the left-hand side of the image is the highest one, and from there steps are continuously directed downwards towards the right-hand side of the image. This way the off-orientation of the sample is compensated. Frequently steps bunch, but small step heights are also observed. Altogether, this image looks like the typical STM image of a vicinal low-index surface. The STM image of a smaller area in Fig. 4(b) reveals that on the terraces dark lines are running from the lower left to the upper right. On this scale there are not any islands visible, either, apart from a few contaminations.

A high-resolution STM image is depicted in Fig. 5. The aforementioned dark lines are indicated by black markers at the borders of the image. Between these lines along $[2\bar{3}1]$, series of three humps are visible that are oriented roughly along $[45\bar{3}]$. The right-hand side of these series lies higher than the left-hand side, and series on neighboring stripes are shifted with respect to each other in direction $[2\bar{3}1]$. On the left-hand side of the image, there is also one stripe that is only two humps wide (cf. arrow). Two different unit meshes are indicated that describe the periodicity of the three-hump stripes. The lengths of the unit vectors of unit mesh *A* are ~11 and ~20 Å, and the enclosed angle is ~70°. This is in accord with the diffraction data, so the two-hump stripe is a deviation from the regular surface structure. Apart from this type of perturbation, the surface is remarkably perfect: Locally, there are no vacancies or other small-scale perturbations. This observation holds for all STM images of well-prepared GaAs(2 5 11) samples. The STM images in Figs. 4(b) and 5 show the same features that were observed in Ref. 37. This is the second evidence that the same surface that was discovered in the spherical depressions is now found on a planar sample.

As the nominal orientation of the planar samples was specified by the wafer manufacturer with an uncertainty of only 0.2°, it was now possible to develop a structural model of the surface. Since filled states were detected for the STM images, the humps are most likely arsenic related. The nominal orientation of most samples was (3 7 15). On the basis of the analysis of GaAs(113)$A$–$(8\times1)$ (cf. Fig. 2), arsenic dimers are expected for surfaces in this angular region. Thus it was assumed that the humps correspond to As dimers, and a structural model of GaAs(3 7 15) was modified until agreement with the experimental data was achieved. This way the Miller indices of the new stable GaAs surface were deter-

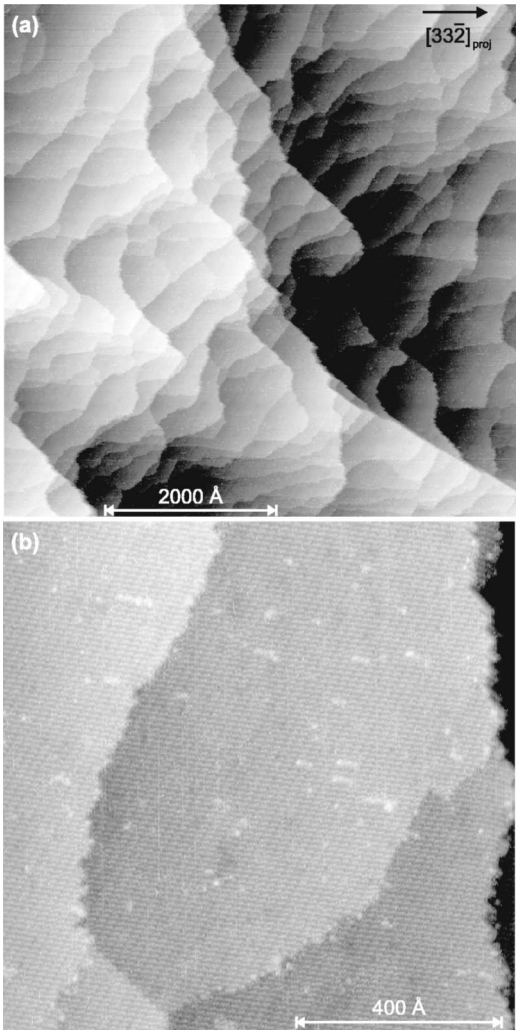


FIG. 4. Overview STM images of GaAs(2 5 11). (a) Large area. $U_{sample}=-2.5$ V, $I=0.1$ nA. (b) Medium size area. $U_{sample}=-2.5$ V, $I=0.13$ nA.

mined as (2 5 11). The experimental uncertainties of the STM and LEED data were irrelevant for the procedure, because the distances between atomic scale features of a crystal can have only discrete values.

The resulting structural model of GaAs(2 5 11) is presented in Fig. 6. Both the unit meshes *A* and *B* are indicated, but the structure is more easily understood by looking at unit mesh *A*. There are three As dimers, three As atoms with one dangling bond each, and seven Ga atoms with one dangling bond each in the unit mesh. On the filled-states STM images the dimers are seen as humps. The dimers are arranged in a series along $[12\bar{1}]$ that is inclined with respect to the surface plane such that the right-hand side lies higher than the left-hand side [cf. cross section in Fig. 6(b)]. Between dimer series that neighbor in direction $[45\bar{3}]$, there is a narrow trench [dashed vertical lines in Fig. 6(a)]. The Ga atoms in these trenches are topographically low, and their dangling bonds are unoccupied, thus they appear as the dark lines on the STM images.

The lengths of the basis vectors of unit mesh *A* are 10.6 and 20.0 Å, and the enclosed angle is 67.8°. All these values are in excellent agreement with the experimental data. The angle between (2 5 11) and the nominal orientation of the samples is 1.0°. The slope and the mean orientation of the steps seen in Fig. 4(a) are in accord with this off-orientation. The angle between [2 5 11], projected into the plane spanned by $[1\bar{1}0]$ and [113], and [113] is 10.0°, which is in good agreement with the experimental value $(9\pm2)°$ that was measured in Ref. 37. The surface structure shown in Fig. 6 fulfills the electron counting rule, i.e., the electrons from the Ga dangling bonds can be distributed in such a way that all the Ga dangling bonds are emptied while all the As dangling bonds are completely filled. Consequently, the surface has a semiconducting ground state. The fulfillment of the ECR is in accord with the experimentally observed stability of the surface.

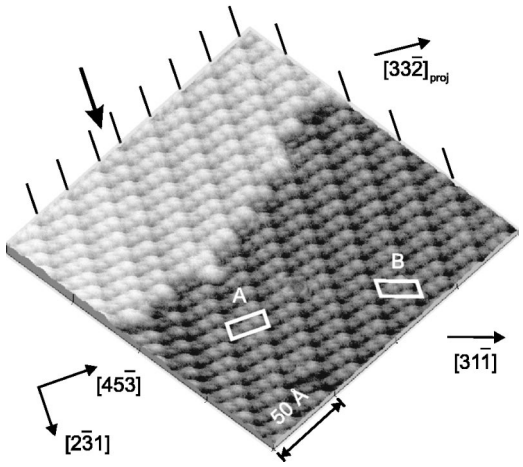


FIG. 5. Three-dimensional STM image of a small area of GaAs(2 5 11). The *z* scale has been magnified. $U_{sample}=-2.5$ V, $I=0.1$ nA.

The complicated structure of this reconstruction can be considered as composed of smaller subunits. The series of three As dimers lies in the (113) plane, as indicated by the dashed parallelogram in Fig. 6(a). GaAs(113)$A$–$(8\times1)$ is a stable surface,[9,10] but the reconstruction does not contain such a series of three As dimers. Hence the occurrence of (113) subunits on GaAs(2 5 11) is not a form of nanofaceting into low-energy surfaces. Note that due to the inclination of the (113) plane with respect to (2 5 11), the dimer bonds are not parallel to the latter plane that forms the stable surface. Such a structural motif of inclined dimer bonds has not been observed on any other GaAs surface.

Dimer series that neighbor in direction $[2\bar{3}1]$ form stripes of the orientation (137) [area between the two vertical dashed lines in Fig. 6(a), see also cross section in Fig. 6(b)]. These stripes are easily recognizable on the STM images. The (137) stripes are not the result of nanofaceting, either, as will be explained in the following. First, the spherical depressions studied in Ref. 37 contained also regions of the mean orientation (137). However, no stable surface was found there. Second, GaAs(137) reconstructed according to the stripes on GaAs(2 5 11) would violate the ECR [the resulting unit mesh is indicated by the dotted parallelogram in Fig. 6(a)]. Therefore it appears unlikely that GaAs(137) is a

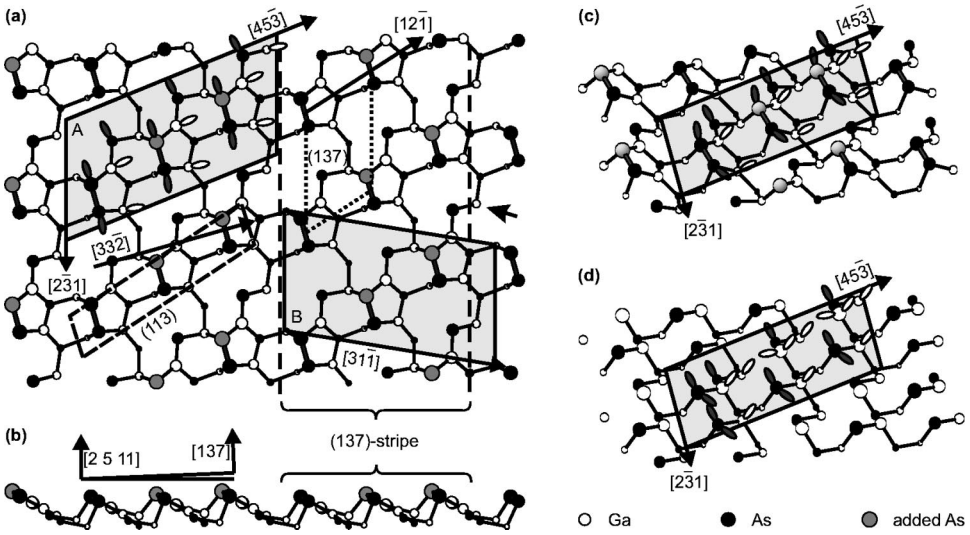


FIG. 6. Structural models of the GaAs(2 5 11) surface. The solid parallelograms indicate the unit mesh. The exact positions of the atoms are the result of the calculations described in the text. The size of the circles representing the atoms was chosen according to their vertical distance from the uppermost atom. To arrive at the reconstructed surface, the lighter shaded As atoms have to be added to the bulk-terminated surface. (a) $(1\times1)$ reconstruction, top view. (b) $(1\times1)$ reconstruction, side view. (c) $(1\times1)$ reconstruction, perspective view. (d) bulk truncated, perspective view.

surface of lower energy than GaAs(2 5 11), although it should be noted that this argument will be weakened by further results presented below. Instead, the stability of the reconstructed GaAs(2 5 11) surface is the result of the balance between (137) stripes of a certain width and the trenches in between: In the trenches there is one Ga dangling bond per unit mesh [cf. arrow on the right-hand side of Fig. 6(a)]. The charge contributed by this dangling bond is exactly necessary to make the complete structure fulfill the ECR.

A model of the bulk-truncated GaAs(2 5 11) surface is shown in Fig. 6(d). In every atomic layer there is an equal number of Ga and As atoms. Thus the surface is stoichiometric. All stoichiometric GaAs surfaces automatically fulfill the ECR. However, there are several atoms with two dangling bonds each, which is energetically very unfavorable. Hence it is unlikely that this structure is stable. The differences between the reconstructed surface [Figs. 6(a)–(c)] and the bulk-truncated surface [Fig. 6(d)] are that two As atoms were added and that the number of dangling bonds was reduced by dimerization of neighboring As atoms. The addition of As atoms in the model is in agreement with the fact that the experimental surface preparation was As rich. The dimerization is in accord with the general principle that the number of dangling bonds at a surface should be small. The periodicity of the reconstruction remains $(1\times1)$, as observed by LEED and RHEED (because of the large bulk-truncated unit mesh, on some high-index surfaces bonds can be created and broken without a change of the periodicity).

The analysis of the experimental data was complemented by first-principles electronic structure calculations. The surface free energy at zero temperature of the reconstructed GaAs(2 5 11) surface was determined as $53\ \mathrm{meV/\AA^2} + 0.0107\ \mathrm{\AA^{-2}}\times(E_{\mathrm{As}}^{coh}-\mu_{\mathrm{As}})$, as depicted in Fig. 7. In the same diagram, the corresponding data for the lowest-energy reconstructions of the well-known GaAs(001) surface are indicated by the gray-shaded area. Although a direct comparison of the surface free energies of surfaces of different crystallographic orientation is not reasonable, it is clear that for As-rich conditions the value for GaAs(2 5 11) ($53\ \mathrm{meV/\AA^2}$) lies well in the range of low-index singular surfaces. Therefore, the theoretical calculations support the proposed structural model.

The interpretation of STM images is not straightforward, because the image is influenced not only by the topography, but also by the electronic structure of the surface. In order to support the interpretation of the experimental STM images, simulated images using the calculated geometry of GaAs(2 5 11) were generated. Experimental high-resolution STM images and the corresponding simulated images are presented in Fig. 8. Both filled and empty states images show elongated humps at three different height levels. Among the experimental images, the resolution of the empty states image is inferior. This corresponds to the empirical fact that it is more difficult to acquire empty states STM images. The main difference between filled and empty states images is which

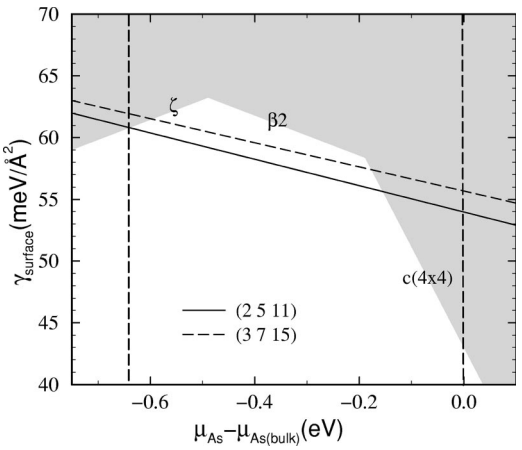


FIG. 7. Calculated surface energies as a function of the chemical potential of arsenic for the GaAs(2 5 11) surface with three As dimers per unit mesh (solid line) and for the GaAs(3 7 15) surface with two As dimers per unit mesh (dashed line). For comparison, surface energies of the GaAs(001) surface for three surface reconstructions ($c(4\times4)$, $\beta2(2\times4)$, and $\zeta(4\times2)$], which have the lowest energies of the presently known reconstructions of GaAs(001), are indicated by the shaded region.

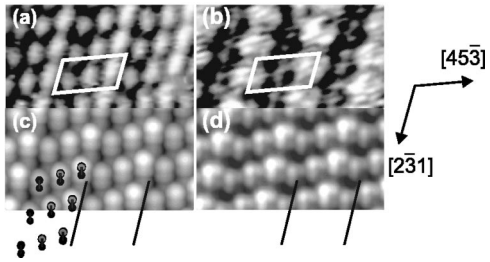


FIG. 8. Experimental and simulated high-resolution STM images of GaAs(2 5 11). The white parallelograms indicate the unit mesh, and the black lines at the bottom mark the dark lines on the images. (a) Experimental, filled states. $U_{sample}=-2.5$ V, $I=0.1$ nA. (b) Experimental, empty states. $U_{sample}=+2.5$ V, $I=0.3$ nA. (c) Simulated, filled states. Arsenic dimers of the structural model in overlay. (d) Simulated, empty states. For the simulated images, the local density of states was integrated for an energy interval that extended from the valence band top to $-2.5$ eV below for the filled states image, and from the bottom of the conduction band to 1 eV above for the empty states image, respectively. It should be noted that these values do not necessarily have to be identical to the experimental biases, because the complex tunneling process is influenced by factors that cannot be controlled, e.g., atoms from the restgas that adsorb on the tip. What is essential is the distinction between filled and empty states images.

separation between humps that neighbor in direction [45$\bar{3}$] is most apparent. On the filled states images, the highest and the lowest humps are well separated. Thus in direction [2$\bar{3}$1] a trench is visible that has been described above and that is indicated by the black lines at the bottom of Fig. 8(c). In contrast, on the empty states images, the intensity does not decrease significantly between the highest and the lowest humps. Hence these humps are not well separated. Therefore the trench is seen between the lowest and the middle level humps, as indicated by the black lines at the bottom of Fig. 8(d). This observation holds for both experimental and simulated images. Altogether, experimental and simulated STM images are in excellent agreement, giving further support to our structural model.

The high structural perfection and the extremely small roughness of GaAs(2 5 11) make this surface absolutely comparable to GaAs(001)–$\beta2(2\times4)$, the GaAs surface that is most frequently used as a substrate for heterostructures. One might think that the inclination of the dimer series could make the GaAs(2 5 11) surface unsuitable as a substrate for growth. However, the corrugation between the highest and the lowest dimer is only 0.5 Å, as opposed to 2.8 Å for GaAs(001)-$\beta2(2\times4)$, and the difference in height between the top and the bottom atom with a dangling bond is 2.1 Å, as opposed to 2.8 Å for GaAs(001)–$\beta2(2\times4)$. Thus GaAs(2 5 11) is actually less corrugated than GaAs(001)–$\beta2(2\times4)$. Nevertheless, the inclined geometry of GaAs(2 5 11) may readily enable the incorporation of new atoms, thus facilitating growth on this surface. Also, on the GaAs(001)–$\beta2(2\times4)$ surface there are usually many holes in the size of a few unit meshes.[47] Therefore GaAs(2 5 11) may be a superior substrate for the growth of heterostructures like, e.g., quantum wells.

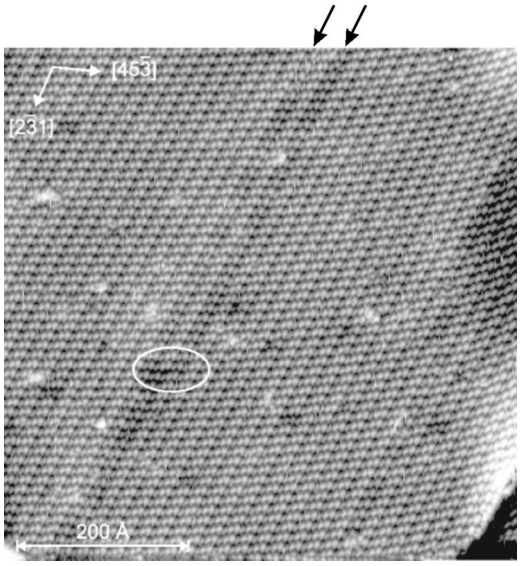


FIG. 9. STM image of GaAs(2 5 11). The arrows at the top image border indicate particularly long two-dimer stripes. The ellipse highlights a location where the widths of two neighboring stripes changes simultaneously. $U_{sample}=-2.6$ V, $I=0.2$ nA.

### B. Line defects

Apart from the regular stripes of the reconstructed GaAs(2 5 11) surface, that are three As dimers wide, the STM images show as well stripes that are two dimers or, seldom, four dimers wide. If such stripes occur, they extend over several 100 Å, as can be seen in Fig. 9. Such two-dimer stripes are indicated by the arrows at the top of the image. Also, the two-dimer stripes cross step edges without changing to the regular three-dimer width (cf. left-hand side of Fig. 5). Thus these stripes are large-scale, ordered perturbations of the surface periodicity. Both the large size and the order indicate that these perturbations are fairly stable. To our knowledge, such a type of surface defect has not been observed on any other surface.

In the following we will focus on the two-dimer stripes, since this type of perturbation is more abundant. A hypothetical surface that consisted exclusively of such two-dimer stripes would have the orientation (3 7 15). The angle between this plane and (2 5 11) is only 1°. Thus the two-dimer stripes can be considered either as line defects of the reconstruction or as minimally off-oriented nanofacets. A structural model of GaAs(3 7 15) is shown in Fig. 10. This is in fact the structure that results from continuously stacking the zigzag dimer chains of the GaAs(113)$A$–$(8\times1)$ reconstruction, as described in the introduction. These zigzag chains are indicated in Fig. 10 by the dotted lines. A two-dimer stripe is marked by the area between the two dashed lines. The unit mesh of the reconstructed GaAs(3 7 15) surface contains two As dimers, two As atoms with one dangling bond each, and five Ga atoms with one dangling bond each. This configuration does not fulfill the ECR; there is an excess of one-quarter of an electron per unit mesh. The violation of the ECR suggests that this surface is of high energy and unstable. However, fairly large areas of this structure occur nevertheless on the stable GaAs(2 5 11) surface, that

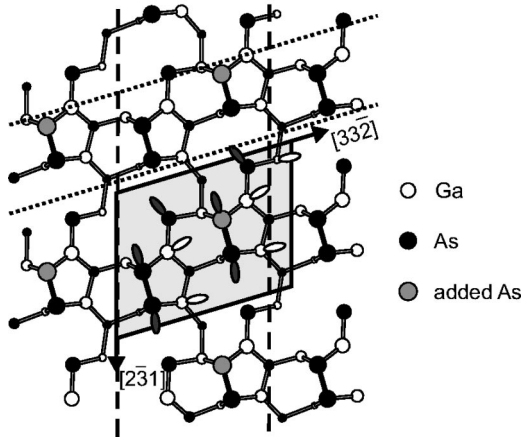


FIG. 10. Structural model of the reconstructed GaAs(3 7 15)–$(1\times1)$ surface in top view. The solid parallelogram indicates the unit mesh. The exact positions of the atoms are the result of the calculations. The size of the circles representing the atoms was chosen according to their vertical distance from the uppermost atom. To arrive at the reconstructed surface, the lighter shaded As atoms have to be added to the bulk-terminated surface.

*does* fulfill the ECR. Hence the difference in energy between these two surfaces may be not as big as one would initially expect on the basis that one surface fulfills the ECR, and the other one does not.

In fact, in terms of saturation of dangling bonds the two surfaces are remarkably similar. First, they comprise obviously the same structural motifs. Second, quantitatively the dangling-bond density of the reconstructed GaAs(3 7 15) surface is greater by only 0.1% than that of the reconstructed GaAs(2 5 11) surface [absolute values: GaAs(2 5 11) $8.176\times10^{-2}$Å$^{-2}$, GaAs(3 7 15) $8.185\times10^{-2}$Å$^{-2}$, for comparison GaAs(001)–$\beta2(2\times4)$ $7.822\times10^{-2}$Å$^{-2}$]. In order to elucidate this finding, first-principles electronic structure calculations were carried out also for the reconstructed GaAs(3 7 15) surface. At zero temperature the surface free energy of this surface is 55 meV/Å$^2$+0.0097 Å$^{-2}\times(E_{\mathrm{As}}^{coh}-\mu_{\mathrm{As}})$. The respective curve has also been included in Fig. 7. For As-rich conditions, as chosen in the experiments, the energy value for GaAs(3 7 15) (55 meV/Å$^2$) is only insignificantly greater than the one for GaAs(2 5 11) (53 meV/Å$^2$). In addition, the calculations show that the valence band is not completely filled on the GaAs(3 7 15) surface, as implied by its violation of the ECR. The unique simultaneous observation of these two structures that differ only with respect to fulfillment of the ECR allows an evaluation of the relative relevance of two important principles for the structure of semiconductor surfaces: It appears that the energy gain arising from the minimization of the number of dangling bonds is significantly greater than the gain arising from reaching a semiconducting ground state. It is suggested that this holds for semiconductor surfaces in general. Therefore structural models for unknown reconstructions that violate the ECR should not be excluded *a priori*, as it is commonly done.

The orientation that corresponds to the four-dimer stripes is (5 13 29). This surface structure violates the ECR, too. Thus similar conclusions may be drawn.

Compound semiconductor surface structures that violate the ECR have been found before.[48,49,52–55] However, on GaSb(001) (Ref. 48) and on GaN(0001) (Ref. 49) this violation is accompanied by a significant enrichment of one of the components at the surface (Sb and Ga, respectively). Thus the composition at the surface deviates significantly from the one in the bulk. As a matter of fact, the basis for the ECR are the different energies of the $sp^3$-hybrid orbitals as they occur in the bulk compound.[8] Hence in the case of one or even more complete layers of one of the components on the surface, a violation of the ECR is not so surprising. In the heteroepitaxial reconstruction Sb/GaAs(111)B,[54,55] the violation of the ECR seems to be induced by the strain contribution to the surface free energy. The only known GaAs reconstruction which has been questioned to fulfill the ECR is the GaAs$(\bar{1}\,1\,\bar{1})$–$(\sqrt{19}\times\sqrt{19})$ reconstruction.[50–53] Structural models have been suggested for this surface on the basis of Auger analysis,[50] STM,[51] calculations in the tight-binding approximation,[52] and x-ray Auger analysis.[53] It was pointed out already that a unit cell with an odd number of atomic sites presents an inherent difficulty to fulfill the ECR.[53] Furthermore, in view of the large size of the unit cell, the charge imbalance in the proposed models is relatively small. Nevertheless, this case remains unresolved. In the case of GaAs(2 5 11)/(3 7 15) a significant deviation from the bulk composition does not occur at the surface. Moreover, these two surface structures are very similar so that differences in strain can be excluded. Thus the only difference left is that one fulfills the ECR and the other one does not. The present study does indeed give interesting insight into the nature of compound semiconductor surfaces.

For completeness it should be noted that for elemental semiconductors similar conclusions have already been drawn. Despite the general principle that surfaces of semiconductors tend to have a semiconducting band structure as well, one of the most famous surface reconstructions, Si(111)–$(7\times7)$, is metallic.[56] Also, first-principles calculations for Si(001)–$(2\times1)$ showed that the major part of the reduction in surface energy compared to the bulk-truncated surface is achieved by dimerization, yielding the saturation of dangling bonds. This process causes a gain in energy of 1.8 eV, while the dimer buckling that makes the surface semiconducting contributes only an energy difference of 0.17 eV.[57] As a consequence of the small energy difference associated with buckling, it is possible to observe both asymmetric and symmetric $(2\times1)$ domains coexisting on the Si(001) surface under suitable conditions.[58] Similarly, we observe on the GaAs(2 5 11) surface a coexistence of two almost degenerate local structures.

Given the small difference in energy between GaAs(2 5 11) and GaAs(3 7 15), the occurrence of the two-dimer stripes is easily understood. This energy difference lies well below the thermal energy available during growth. Therefore entropic considerations alone make the occurrence of the two-dimer stripe probable. In addition, the two structures are very similar, so the formation of a two-dimer series instead of the regular three-dimer one is fairly probable. A single two-dimer series, surrounded by three-dimer series, would give rise to domain boundaries with additional dan-

gling bonds. In contrast, the borders between a two-dimer stripe and the neighboring three-dimer stripes are indistinguishable from the borders between neighboring three-dimer stripes. Thus a whole stripe of two-dimer series develops. Once a two-dimer stripe has formed, it is stabilized kinetically: In order to turn it into a three-dimer stripe, all the neighboring stripes on the whole terrace would have to be shifted. This would necessitate a significant structural change across the *whole terrace* in direction $[45\bar{3}]$. While the required long-range mass transport is difficult to achieve, local rearrangements are more probable. Indeed, one can experimentally observe that two-dimer stripes change into three-dimer stripes, but only if the neighboring three-dimer stripe changes at the same location into a two-dimer stripe. This can be seen in Fig. 9 (cf. ellipse).

Some of the studied samples are of the nominal orientation (3 7 15). Hence one may suspect that the occurrence of the two-dimer stripes is due to the macroscopic off-orientation from the direction (2 5 11). However, the overview STM images show that this off-orientation is mostly compensated by well-resolved steps, and not by the two-dimer stripes. Also, such stripes were observed also on the samples that were off-oriented in a different direction. Moreover, four-dimer-wide stripes were also found on the (3 7 15) samples. Four-dimer stripes cause in fact a change in orientation in the opposite direction than the macroscopic off-orientation of the samples. Therefore we conclude that the occurrence of stripes of a different width is an intrinsic perturbation of the GaAs(2 5 11) surface.

Finally, we would like to add an interesting speculation. According to our calculations, GaAs(3 7 15) is weakly metallic. Thus the thin stripes of this orientation that are embedded in the semiconducting GaAs(2 5 11) surface could possibly be electronically one-dimensional systems. Therefore an experimental study on the electronic structure of GaAs(2 5 11) is desirable.

### C. Annealing in ultrahigh vacuum

For GaAs(001) it is well known that, depending on the preparation conditions, different reconstructions form at the surface.[59,60] Thus in addition to varying the growth parameters, GaAs(2 5 11) surfaces that had previously been prepared by MBE were annealed in ultrahigh vacuum. As arsenic desorbs at a lower temperature than gallium, this preparation method usually yields gallium-rich structures.

A LEED image of the resulting surface is shown in Fig. 11. The background intensity is higher than on the image taken after MBE preparation [cf. Fig. 3(a)], and fewer spots are visible. The diffraction pattern is clearly different: Prior to annealing in UHV, there are rows of neighboring particularly bright spots along $[7\bar{5}1]$ and $[19\,10\,\bar{8}]$. In contrast, in Fig. 11 there are rows of bright spots along directions that lie close to $[\bar{1}6\,35\,\bar{1}3]$ and $[19\,10\,\bar{8}]$. Also, many spots of the complete diffraction pattern are not visible. The separations of the spots are different, too. The lengths of the unit mesh $C$ that is marked in Fig. 11 are in real space $11.0\pm0.5$ Å and $27.5\pm1.4$ Å, and the enclosed angle is $84°\pm4°$.

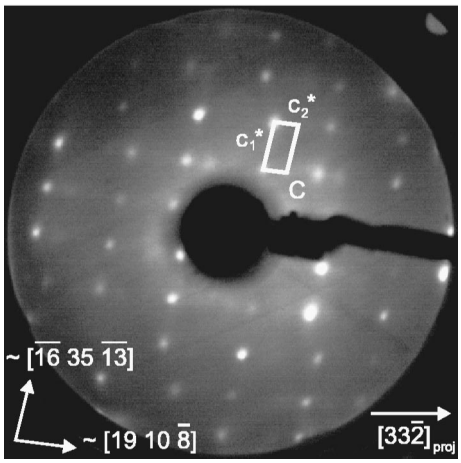


FIG. 11. LEED image of the GaAs(2 5 11) surface after annealing in UHV. $E=57$ eV.

An overview STM image of the UHV annealed surface is presented in Fig. 12. Step edges that are fairly straight for typically about 1000 Å extend from the upper left to the lower right, e.g., as a continuation of the white arrow in Fig. 12. However, these straight step edges do not meet other step edges but end in regions of even gray level, i.e., constant average height. Thus there are not any extended terraces as opposed to Fig. 4(a), the surface is automatically more rough. Steps decline from the bottom left-hand part of the image towards the top right-hand part of the image. Therefore both the orientation of the step edges and of the mean slope of the surface are different than prior to annealing in UHV.

A higher resolution reveals that on the surface there are rows of humps running from the upper left to the lower right [Fig. 13(a)]. The different gray levels suggest that the humps belong to different layers. However, steps are clearly visible only at two locations [cf. arrows in Fig. 13(a)]. Throughout the rest of the image, there seems to be an irregular up and down of adjacent humps. Thus there are not any extended terraces. These features can also be seen on the STM image

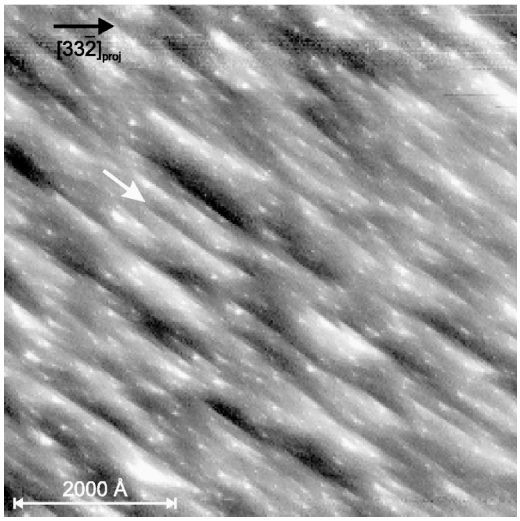


FIG. 12. Overview STM image of the GaAs(2 5 11) surface after annealing in UHV. $U_{sample}=-2.5$ V, $I=0.3$ nA.

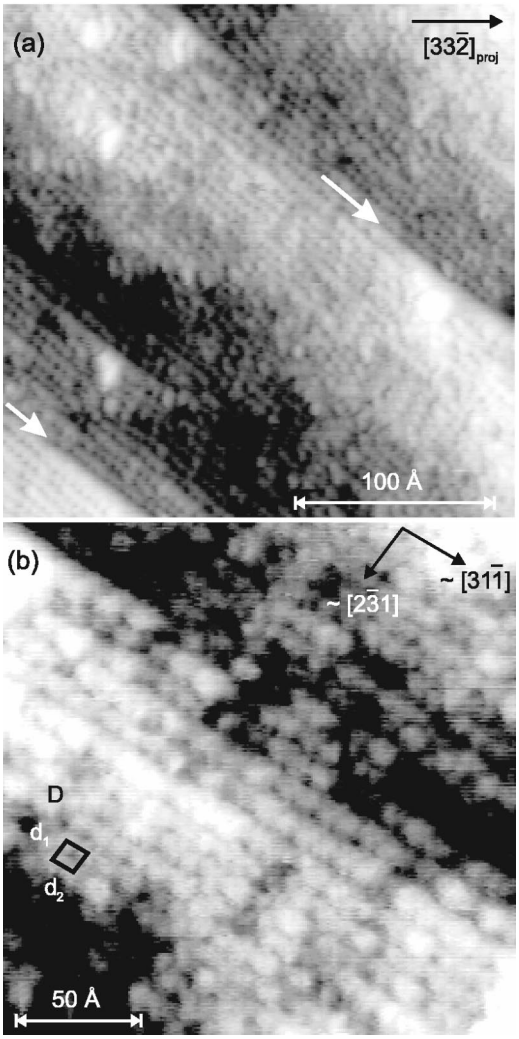


FIG. 13. STM images of the GaAs(2 5 11) surface after annealing in UHV. (a) Medium size area. $U_{sample}=-2.5$ V, $I=0.1$ nA. (b) Small area. $U_{sample}=-2.5$ V, $I=0.1$ nA.

of a small area in Fig. 13(b). On this image a unit mesh is indicated that is almost squared. However, a periodic arrangement of the humps can be found only for areas that have the size of only a few unit meshes. Thus the measurements of the unit mesh cannot be determined with high accuracy. The lengths of the unit vectors $d_1$ and $d_2$ are $\sim 11$ and $\sim 10$ Å, respectively, and the enclosed angle is $\sim 90°$. The orientations of these unit vectors and the length of $d_1$ are in fairly good agreement with the LEED data, but $d_2$ is significantly smaller than $c_2$.

The high background intensity of the LEED image indicates that the surface is poorly ordered. This conclusion is confirmed by the STM images that show a rough surface with very small domains of periodic structures. However, the absence of spot splitting in LEED and of well evolved inclined areas in STM suggests that the surface does not decay into facets of surfaces of other orientation.

The unit meshes of the UHV annealed surface and of GaAs(2 5 11) are incommensurate. Thus it is unlikely that during annealing a different reconstruction of this orientation evolves. Instead, we suppose that areas of a nearby surface form that is under Ga-rich conditions energetically more favorable than GaAs(2 5 11). This conclusion is corroborated by the observation that the average step direction and the mean slope of the surface change during annealing. Hence planar regions are in a different direction off-oriented with respect to the nominal sample orientation than it is the case for GaAs(2 5 11). However, because of the high degree of roughness, such planar regions are small.

Different unit meshes were extracted from the LEED and STM data of the UHV annealed surface. When the experimental uncertainties are taken into account, it holds $c_1 \approx d_1$ and $c_2 \approx 3d_2$. There could be two reasons for this inconsistency. First, the humps in the STM images could be related to different structural elements that cannot be distinguished due to the limited resolution. In this case only every third hump would be actually equivalent. Second, there could be a small shift after every third hump that is not recognizable in the STM images because the ordered domains are so small. Thus these shifts would not be distinguishable from the ubiquitous defects.

Because of the high degree of disorder on the surface, it is difficult to construct a structural model and assign the humps in the STM images to structural elements. Bright features in filled states images of GaAs are usually related to arsenic states. Indeed, both the length and the orientation with respect to $[33\bar{2}]_{proj}$ of $c_1 \approx 11$ Å $\approx d_1$ are in good accord with those of $a_1=10.6$ Å on GaAs(2 5 11). Thus the humps on the STM images of the UHV annealed surface could also be due to arsenic dimers. The occurrence of arsenic dimers on a surface that was prepared under Ga-rich conditions may seem surprising. However, the GaAs(114)$A-\alpha 2(2\times 1)$ reconstruction, which forms after a similar preparation, also contains arsenic dimers.[20] Anyhow, an arrangement of arsenic dimers that would be in accord with the experimental unit vectors is not possible near the (2 5 11) plane. Hence at least some of the humps are related to a different structural motif.

## IV. CONCLUSIONS

GaAs(2 5 11) is a stable compound semiconductor surface located *within* the stereographic triangle. After preparation by MBE, a $(1\times 1)$ reconstruction is observed whose characteristic structural element is a series of three As dimers that is inclined with respect to the surface plane. On a mesoscopic scale, the surface morphology is similar to that of low-index surfaces. The surface free energy falls well into the range of those of low-index surfaces. The surface periodicity of GaAs(2 5 11) is perturbed by thin stripes that belong to the orientation (3 7 15). The analysis of this regular perturbation suggests that, in general, on semiconductor surfaces the gain in stability arising from the minimization of the number of dangling bonds is significantly greater than the gain arising from reaching a semiconducting ground state. Annealing in UHV yields a fairly rough surface whose mean orientation is different from (2 5 11).

**ACKNOWLEDGMENTS**

We are grateful to T. Suzuki for helpful discussions. We would like to thank M. Scheffler and G. Ertl for support and P. Geng for technical assistance. Figures 6 and 10 were produced with the help of BALSAC (version 2.12, © K. Hermann 1991–9). This work was supported by the Deutsche Forschungsgemeinschaft (Sonderforschungsbereich 296) and by the German Bundesministerium für Bildung und Forschung under Grant No. 05 622 EBA4.

*Corresponding author.
Electronic address: jacobi@fhi-berlin.mpg.de

[1] M. J. Kelly, *Low-Dimensional Semiconductors* (Oxford University Press, Oxford, 1995); H. Asahi, Adv. Mater. **9**, 1019 (1997); D. Bimberg, M. Grundmann, and N. N. Ledentsov, *Quantum Dot Heterostructures* (Wiley, Chichester, 1999), and references therein.

[2] M. Grundmann, Physica E (Amsterdam) **5**, 167 (2000), and references therein.

[3] J.M. Moison, F. Houzay, F. Barthe, L. Leprince, E. André, and O. Vatel, Appl. Phys. Lett. **64**, 196 (1994); Y. Nabetani, T. Ishikawa, S. Noda, and A. Sasaki, J. Appl. Phys. **76**, 347 (1994); A. Gustafsson, F. Reinhardt, G. Biasiol, and E. Kapon, Appl. Phys. Lett. **67**, 3673 (1995); R.P. Mirin, J.P. Ibbetson, K. Nishi, A.C. Gossard, and J.E. Bowers, *ibid.* **67**, 3795 (1995); G. Biasiol, F. Reinhardt, A. Gustafsson, and E. Kapon, *ibid.* **71**, 1831 (1997); X.-L. Wang, M. Ogura, H. Matsuhata, and A. Hamoudi, *ibid.* **71**, 2130 (1997); B.A. Joyce, T.S. Jones, and J.G. Belk, J. Vac. Sci. Technol. B **16**, 2373 (1998); E. Kapon, F. Reinhardt, G. Biasiol, and A. Gustafsson, Appl. Surf. Sci. **123/124**, 674 (1998); X.-L. Wang, V. Voliotis, R. Grousson, and M. Ogura, J. Cryst. Growth **213**, 19 (2000).

[4] H. Lee, R. Lowe-Webb, W. Yang, and P.C. Sercel, Appl. Phys. Lett. **72**, 812 (1998).

[5] Y. Hasegawa, H. Kiyama, Q.K. Xue, and T. Sakurai, Appl. Phys. Lett. **72**, 2265 (1998).

[6] J. Márquez, L. Geelhaar, and K. Jacobi, Appl. Phys. Lett. **78**, 2309 (2001).

[7] C.B. Duke, Chem. Rev. **96**, 1237 (1996).

[8] W.A. Harrison, J. Vac. Sci. Technol. **16**, 1492 (1979); M.D. Pashley, Phys. Rev. B **40**, 10 481 (1989).

[9] M. Wassermeier, J. Sudijono, M.D. Johnson, K.T. Leung, B.G. Orr, L. Däweritz, and K. Ploog, Phys. Rev. B **51**, 14 721 (1995).

[10] J. Platen, A. Kley, C. Setzer, K. Jacobi, P. Ruggerone, and M. Scheffler, J. Appl. Phys. **85**, 3597 (1999).

[11] L. Geelhaar, J. Márquez, and K. Jacobi, Phys. Rev. B **60**, 15 890 (1999).

[12] A. Richter, G. Behme, M. Süptitz, C. Lienau, T. Elsaesser, M. Ramsteiner, R. Notzel, and K.H. Ploog, Phys. Rev. Lett. **79**, 2145 (1997).

[13] R. Nötzel, Z. Niu, M. Ramsteiner, H.-P. Schönherr, A. Trampert, L. Däweritz, and K.H. Ploog, Nature (London) **392**, 56 (1998).

[14] C. Herring, in *Structure and Properties of Solid Surfaces* (University Press, Chicago, 1953), pp. 5–72.

[15] W. Braun, O. Brandt, M. Wassermeier, L. Däweritz, and K. Ploog, Appl. Surf. Sci. **104**, 35 (1996); C. Setzer, J. Platen, P. Geng, W. Ranke, and K. Jacobi, Surf. Sci. **377-379**, 125 (1997); P. Moriarty, Y.-R. Ma, A.W. Dunn, P.H. Beton, M. Henini, C. McGinley, E. McLoughlin, A.A. Cafolla, G. Hughes, S. Downes, D. Teehan, and B. Murphy, Phys. Rev. B **55**, 15 397 (1997); M. Pristovsek, H. Menhal, T. Wehnert, J.-T. Zettler, T. Schmidtling, N. Esser, W. Richter, C. Setzer, J. Platen, and K. Jacobi, J. Cryst. Growth **195**, 1 (1998).

[16] M. Kawase, Y. Ishikawa, and T. Fukui, Appl. Surf. Sci. **130-132**, 457 (1998); M. Pristovsek, H. Menhal, T. Schmidtling, N. Esser, and W. Richter, Microelectron. J. **30**, 449 (1999).

[17] J. Márquez, L. Geelhaar, and K. Jacobi, Phys. Rev. B **62**, 9969 (2000).

[18] S. Shimomura, A. Wakejima, A. Adachi, Y. Okamoto, N. Sano, K. Murase, and S. Hiyamizu, Jpn. J. Appl. Phys., Part 2 **32**, L1728 (1993); Y. Tsuda, S. Shimomura, S. Hiyamizu, and N. Sano, J. Cryst. Growth **150**, 415 (1995); T. Yamada, H. Yamaguchi, and Y. Horikoshi, *ibid.* **150**, 421 (1995); H. Yamaguchi, T. Yamada, and Y. Horikoshi, Jpn. J. Appl. Phys., Part 2 **34**, L1490 (1995).

[19] J. Platen, C. Setzer, W. Ranke, and K. Jacobi, Appl. Surf. Sci. **123/124**, 43 (1998).

[20] J. Márquez, P. Kratzer, L. Geelhaar, K. Jacobi, and M. Scheffler, Phys. Rev. Lett. **86**, 115 (2001).

[21] R. Notzel, N.N. Ledentsov, L. Daweritz, M. Hohenstein, and K. Ploog, Phys. Rev. Lett. **67**, 3812 (1991).

[22] R. Nötzel, L. Däweritz, and K. Ploog, Phys. Rev. B **46**, 4736 (1992).

[23] W. Weiss, W. Ranke, D. Schmeisser, and W. Göpel, Surf. Sci. **221**, 91 (1989).

[24] S. Horng, K. Young, and A. Kahn, J. Vac. Sci. Technol. A **7**, 2039 (1989).

[25] H.-P. Schönherr, J. Fricke, Z. Niu, K.-J. Friedland, R. Nötzel, and K.H. Ploog, Appl. Phys. Lett. **72**, 566 (1998).

[26] R. Nötzel, D. Eissler, M. Hohenstein, and K. Ploog, J. Appl. Phys. **74**, 431 (1993).

[27] J. Platen, C. Setzer, P. Geng, W. Ranke, and K. Jacobi, Microelectron. J. **28**, 969 (1997); L. Geelhaar, J. Márquez, K. Jacobi, A. Kley, P. Ruggerone, and M. Scheffler, *ibid.* **30**, 393 (1999); K. Jacobi, J. Platen, C. Setzer, J. Márquez, L. Geelhaar, C. Meyne, W. Richter, A. Kley, P. Ruggerone, and M. Scheffler, Surf. Sci. **439**, 59 (1999).

[28] T.T. Tsong, D.Ł. Feng, and H.M. Liu, Surf. Sci. **199**, 421 (1988).

[29] Z. Gai, R.G. Zhao, H. Ji, X. Li, and W.S. Yang, Phys. Rev. B **56**, 12 308 (1997).

[30] Z. Gai, R.G. Zhao, and W.S. Yang, Phys. Rev. B **57**, R6795 (1998).

[31] Z. Gai, X. Li, R.G. Zhao, and W.S. Yang, Phys. Rev. B **57**, R15 060 (1998).

[32] Z. Gai, W.S. Yang, R.G. Zhao, and T. Sakurai, Phys. Rev. B **59**, 15 230 (1999).

[33] S.C. Erwin, A.A. Baski, and L.J. Whitman, Phys. Rev. Lett. **77**, 687 (1996).

[34] L. Geelhaar, Ph.D. thesis, Technical University of Berlin, 2000.

[35] K. Jacobi, L. Geelhaar, and J. Márquez, Appl. Phys. A: Mater. Sci. Process., DPG spring meeting, Hamburg, Germany (to be published).

[36] N. Moll, M. Scheffler, and E. Pehlke, Phys. Rev. B **58**, 4566 (1998); L.G. Wang, P. Kratzer, N. Moll, and M. Scheffler, *ibid.*

**62**, 1897 (2000), and references therein.
[37] L. Geelhaar, J. Márquez, and K. Jacobi, Phys. Rev. B **62**, 6908 (2000).
[38] L. Geelhaar, J. Márquez, P. Kratzer, and K. Jacobi, Phys. Rev. Lett. **86**, 3815 (2001).
[39] P. Geng, J. Márquez, L. Geelhaar, J. Platen, C. Setzer, and K. Jacobi, Rev. Sci. Instrum. **71**, 504 (2000).
[40] M. Bockstedte, A. Kley, J. Neugebauer, and M. Scheffler, Comput. Phys. Commun. **107**, 187 (1997).
[41] M. Fuchs and M. Scheffler, Comput. Phys. Commun. **116**, 67 (1999).
[42] J.P. Perdew and A. Zunger, Phys. Rev. B, **23**, 5048 (1981).
[43] K. Shiraishi, J. Phys. Soc. Jpn. **10**, 3455 (1990).
[44] H.J. Monkhorst and J.D. Pack, Phys. Rev. B **13**, 5188 (1976).
[45] J. Tersoff and D.R. Hamann, Phys. Rev. B **31**, 805 (1985).
[46] N. Moll, A. Kley, E. Pehlke, and M. Scheffler, Phys. Rev. B **54**, 8844 (1996).
[47] See, e.g., A.R. Avery, D.M. Holmes, T.S. Jones, B.A. Joyce, and G.A.D. Briggs, Phys. Rev. B **50**, 8098 (1994); T. Hashizume, Y.-K. Xue, A. Ichimiya, and T. Sakurai, *ibid.* **51**, 4200 (1995); A.R. Avery, C.M. Goringe, D.M. Holmes, J.L. Sudijono, and T.S. Jones, Phys. Rev. Lett. **76**, 3344 (1996).
[48] L.J. Whitman, P.M. Thibado, S.C. Erwin, B.R. Bennett, and B.V. Shanabrook, Phys. Rev. Lett. **79**, 693 (1997).
[49] A.R. Smith, R.M. Feenstra, D.W. Greve, M.S. Shin, M. Skowronski, J. Neugebauer, and J.E. Northrup, J. Vac. Sci. Technol. B **16**, 2242 (1998).
[50] K. Jacobi, C.v. Muschwitz, and W. Ranke, Surf. Sci. **82**, 270 (1979).
[51] D.K. Biegelsen, R.D. Bringans, J.E. Northrup, and L.-E. Swartz, Phys. Rev. Lett. **65**, 452 (1990).
[52] M. Haugk, J. Elsner, M. Sternberg, and Th. Frauenheim, J. Phys.: Condens. Matter **10**, 4523 (1998).
[53] H.H. Farrell, Jun Lu, B.D. Schultz, A.B. Denison, and C.J. Palmstrøm, J. Vac. Sci. Technol. B **19**, 1597 (2001).
[54] P. Moriarty, P.H. Beton, M. Henini, and D.A. Woolf, Surf. Sci. **365**, L663 (1996).
[55] R.H. Miwa and G.P. Srivastava, Phys. Rev. B **63**, 125341 (2001).
[56] F.J. Himpsel, D.E. Eastman, P. Heimann, B. Reihl, C.W. White, and D.M. Zehner, Phys. Rev. B **24**, 1120 (1981).
[57] A. Ramstad, G. Brocks, and P.J. Kelly, Phys. Rev. B **51**, 14 504 (1995).
[58] T. Yokoyama and K. Takayanagi, Phys. Rev. B **61**, R5078 (2000).
[59] P. Drathen, W. Ranke, and K. Jacobi, Surf. Sci. **77**, L162 (1978).
[60] L. Däweritz and R. Hey, Surf. Sci. **236**, 15 (1990).